Eur. Phys. J. C (2011) 71: 1515
DOI 10.1140/epjc/s10052-010-1515-z

THE EUROPEAN PHYSICAL JOURNAL C

Regular Article - Experimental Physics

Reevaluation of the hadronic contributions to the muon $g-2$ and to $\alpha(M_Z^2)$

M. Davier[1], **A. Hoecker**[2,a], **B. Malaescu**[1,b], **Z. Zhang**[1]

[1]Laboratoire de l'Accélérateur Linéaire, IN2P3/CNRS, Université Paris-Sud 11, Orsay, France
[2]CERN, 1211, Geneva 23, Switzerland

Received: 21 October 2010 / Revised: 26 November 2010 / Published online: 5 January 2011

Abstract We reevaluate the hadronic contributions to the muon magnetic anomaly, and to the running of the electromagnetic coupling constant at the Z-boson mass. We include new $\pi^+\pi^-$ cross-section data from KLOE, all available multi-hadron data from BABAR, a reestimation of missing low-energy contributions using results on cross sections and process dynamics from BABAR, a reevaluation of all experimental contributions using the software package HVPTools together with a reanalysis of inter-experiment and inter-channel correlations, and a reevaluation of the continuum contributions from perturbative QCD at four loops. These improvements lead to a decrease in the hadronic contributions with respect to earlier evaluations. For the muon $g-2$ we find lowest-order hadronic contributions of $(692.3\pm4.2)\cdot10^{-10}$ and $(701.5\pm4.7)\cdot10^{-10}$ for the e^+e^--based and τ-based analyses, respectively, and full Standard Model predictions that differ by 3.6σ and 2.4σ from the experimental value. For the e^+e^--based five-quark hadronic contribution to $\alpha(M_Z^2)$ we find $\Delta\alpha^{(5)}_{\rm had}(M_Z^2)=(274.9\pm1.0)\cdot10^{-4}$. The reduced electromagnetic coupling strength at M_Z leads to an increase by 12 GeV in the central value of the Higgs boson mass obtained by the standard Gfitter fit to electroweak precision data.

1 Introduction

The Standard Model (SM) predictions of the anomalous magnetic moment of the muon, a_μ, and of the running electromagnetic coupling constant, $\alpha(s)$, are limited in precision by contributions from virtual hadronic vacuum polarisation. The dominant hadronic terms can be calculated with a combination of experimental cross section data, involving e^+e^- annihilation to hadrons, and perturbative QCD. These are used to evaluate an energy-squared dispersion integral, ranging from the $\pi^0\gamma$ threshold to infinity. The integration kernels occurring in the dispersion relations emphasise low photon virtualities, owing to the $1/s$ descend of the cross section, and, in case of a_μ, to an additional $1/s$ suppression. In the latter case, about 73% of the lowest order hadronic contribution is provided by the $\pi^+\pi^-(\gamma)$ final state,[1] while this channel amounts to only 13% of the hadronic contribution to $\alpha(s)$ at $s=M_Z^2$.

In this paper, we reevaluate the lowest-order hadronic contribution, $a_\mu^{\rm had,LO}$, to the muon magnetic anomaly, and the hadronic contribution, $\Delta\alpha_{\rm had}(M_Z^2)$, to the running $\alpha(M_Z^2)$ at the Z-boson mass. We include new $\pi^+\pi^-$ cross-section data from KLOE [1] and all the available multi-hadron data from BABAR [2–9]. We also perform a reestimation of missing low-energy contributions using results on cross sections and process dynamics from BABAR. We reevaluate all the experimental contributions using the software package HVPTools [10], including a comprehensive reanalysis of inter-experiment and inter-channel correlations. Furthermore, we recompute the continuum contributions using perturbative QCD at four loops [11]. These improvements taken together lead to a decrease of the hadronic contributions with respect to our earlier evaluation [10], and thus to an accentuation of the discrepancy between the SM prediction of a_μ and the experimental result [12]. The reduced electromagnetic coupling strength at M_Z leads to an increase in the most probable value for the Higgs boson mass returned by the electroweak fit, thus relaxing the tension with the exclusion results from the direct Higgs searches.

[a] e-mail: Andreas.Hoecker@cern.ch
[b] Now at CERN, 1211, Geneva 23, Switzerland.

[1] Throughout this paper, final state photon radiation is implied for all hadronic final states.

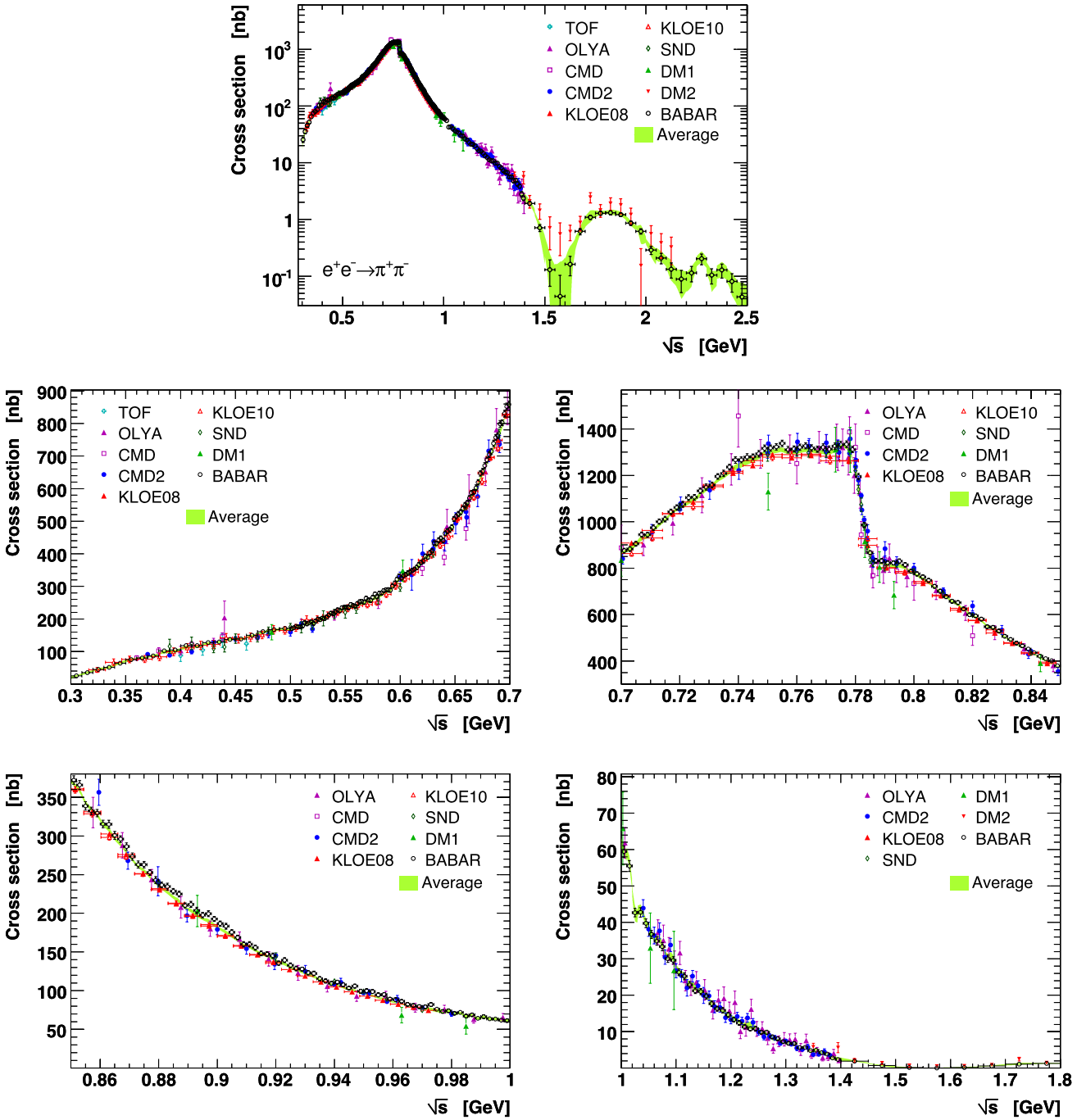

Fig. 1 Cross section of $e^+e^- \to \pi^+\pi^-$ versus centre-of-mass energy for different energy ranges. Shown are data from TOF [17], OLYA [18, 19], CMD [18], CMD2 [20–23], SND [24], DM1 [25], DM2 [26], KLOE [1, 13], and BABAR [2]. The *error bars* show statistical and systematic errors added in quadrature. The *light shaded* (*green*) *band* indicates the HVPTools average within 1σ errors

2 New input data

The KLOE Collaboration has published new $\pi^+\pi^-\gamma$ cross section data with $\pi^+\pi^-$ invariant mass-squared between 0.1 and 0.85 GeV^2 [1]. The radiative photon in this analysis is required to be detected in the electromagnetic calorimeter, which reduces the selected data sample to events with large photon scattering angle (polar angle between 50° and 130°), and photon energies above 20 MeV. The new data are found to be in agreement with, but less precise than, previously published data using small angle photon scattering [13] (superseding earlier KLOE data [14]). They hence exhibit the known discrepancy, on the ρ resonance peak and above, with other $\pi^+\pi^-$ data, in particular those from BABAR,

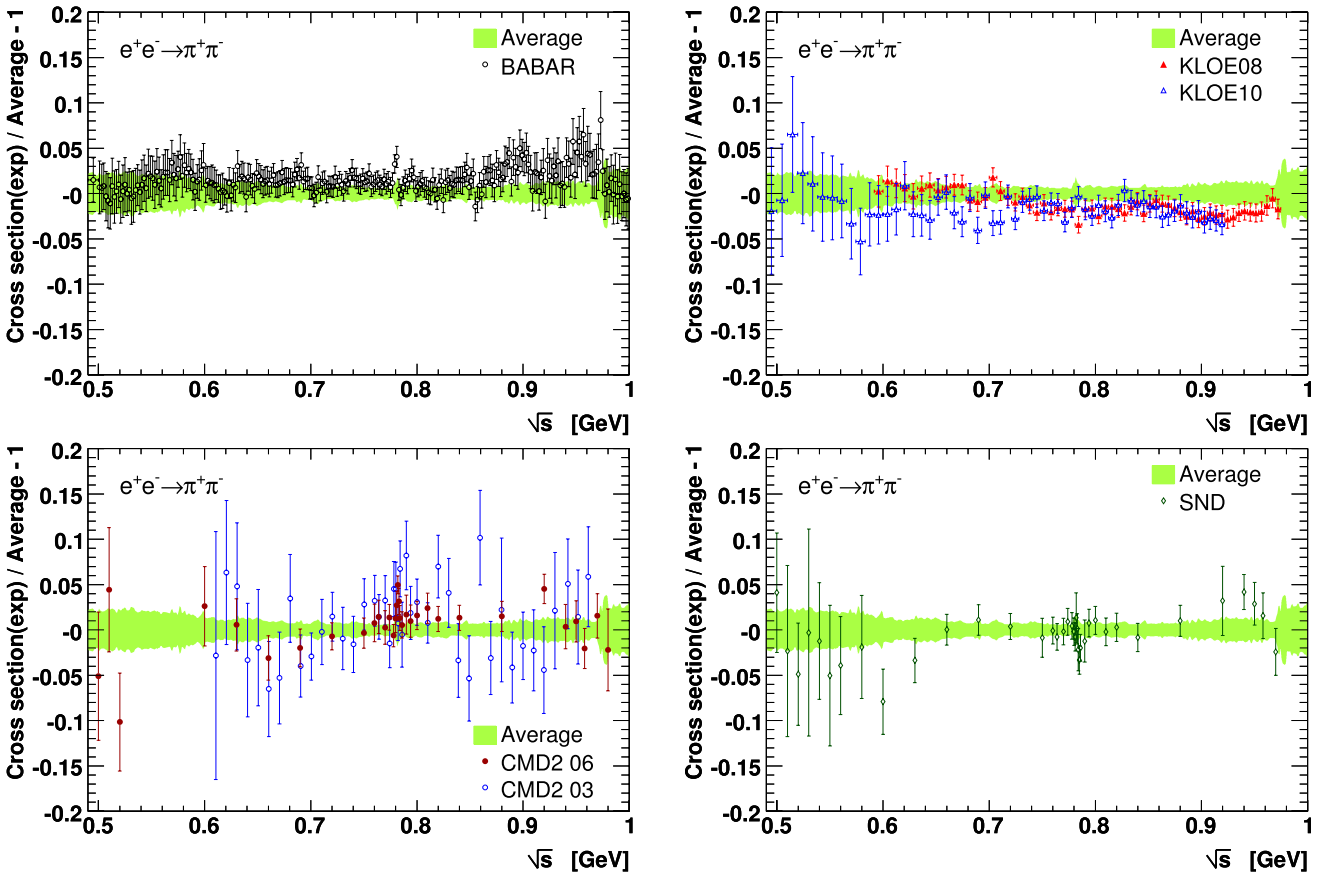

Fig. 2 Comparison between individual $e^+e^- \to \pi^+\pi^-$ cross section measurements from BABAR [2], KLOE 08 [13], KLOE 10 [1], CMD2 03 [20], CMD2 06 [21–23], SND [24], and the HVPTools average. The *error bars* show statistical and systematic errors added in quadrature

obtained using the same ISR technique [2], and with data from $\tau^- \to \pi^-\pi^0\nu_\tau$ decays [15].

Figure 1 shows the available $e^+e^- \to \pi^+\pi^-$ cross section measurements in various panels for different centre-of-mass energies ($\sqrt{s}$). The light shaded (green) band indicates the HVPTools average within $1\,\sigma$ errors. The deviation between the average and the most precise individual measurements is depicted in Fig. 2. Figure 3 shows the weights versus $\sqrt{s}$ the different experiments obtain in the locally performed average. BABAR and KLOE dominate the average over the entire energy range. Owing to the sharp radiator function, the available statistics for KLOE increases towards the ϕ mass, hence outperforming BABAR above ∼0.8 GeV. For example, at 0.9 GeV KLOE's small photon scattering angle data [13] have statistical errors of 0.5%, which is twice smaller than that of BABAR (renormalising BABAR to the 2.75 times larger KLOE bins at that energy). Conversely, at 0.6 GeV the comparison reads 1.2% (KLOE) versus 0.5% (BABAR, again given in KLOE bins which are about 4.2 times larger than for BABAR at that energy). The discrepancy between the BABAR and KLOE data sets above 0.8 GeV causes error rescaling in their average, and hence

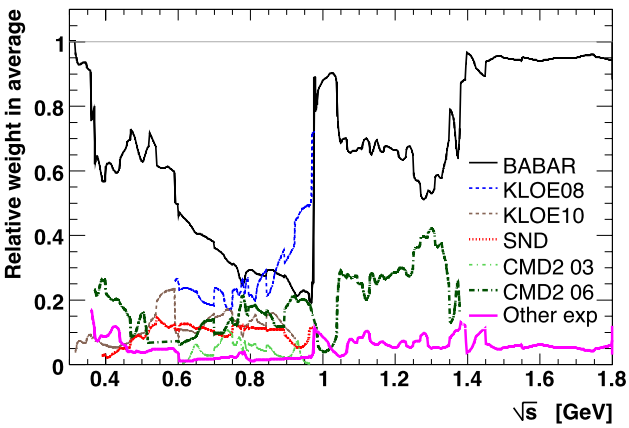

Fig. 3 Relative local averaging weight per experiment versus centre-of-mass energy in $e^+e^- \to \pi^+\pi^-$. See Figs. 1 and 2 for references

loss of precision. The group of experiments labelled "other exp" in Fig. 3 corresponds to older data with incomplete radiative corrections. Their weights are small throughout the entire energy domain. The computation of the dispersion integral over the full $\pi^+\pi^-$ spectrum requires to extend the

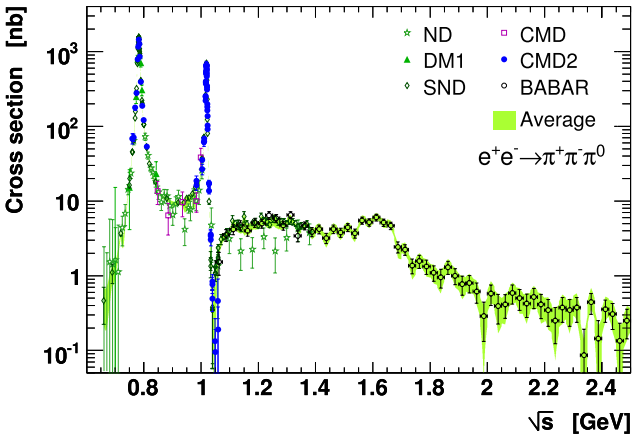

Fig. 4 Cross section of $e^+e^- \to \pi^+\pi^-\pi^0$ versus centre-of-mass energy. Shown are data from ND [27], DM1 [28], SND [29], CMD [30], CMD2 [31] and BABAR [3]. The *error bars* show statistical and systematic errors added in quadrature. The *light shaded* (*green*) *band* indicates the HVPTools average within 1σ errors

available data to the region between threshold and 0.3 GeV, for which we use a fit as described in [10].

We have modified in this work the treatment of the $\omega(782)$ and $\phi(1020)$ resonances, using non-resonant data from BABAR [3]. While in our earlier analyses, the resonances were fitted, analytically integrated, and the non-resonant contributions added separately, we now determine all the dominant contributions directly from the corresponding measurements. Hence the ω and ϕ contributions are included in the $\pi^+\pi^-\pi^0$, $\pi^0\gamma$, $\eta\gamma$, K^+K^-, $K^0_SK^0_L$ spectra. Small remaining decay modes are considered separately. As an example for this procedure, the $e^+e^- \to \pi^+\pi^-\pi^0$ cross section measurements, featuring dominantly the ω and ϕ resonances, are shown in Fig. 4, together with the HVPTools average.

We also include new, preliminary, $e^+e^- \to \pi^+\pi^-2\pi^0$ cross section measurements from BABAR [5], which significantly help to constrain a contribution with disparate experimental information. The available four-pion measurements

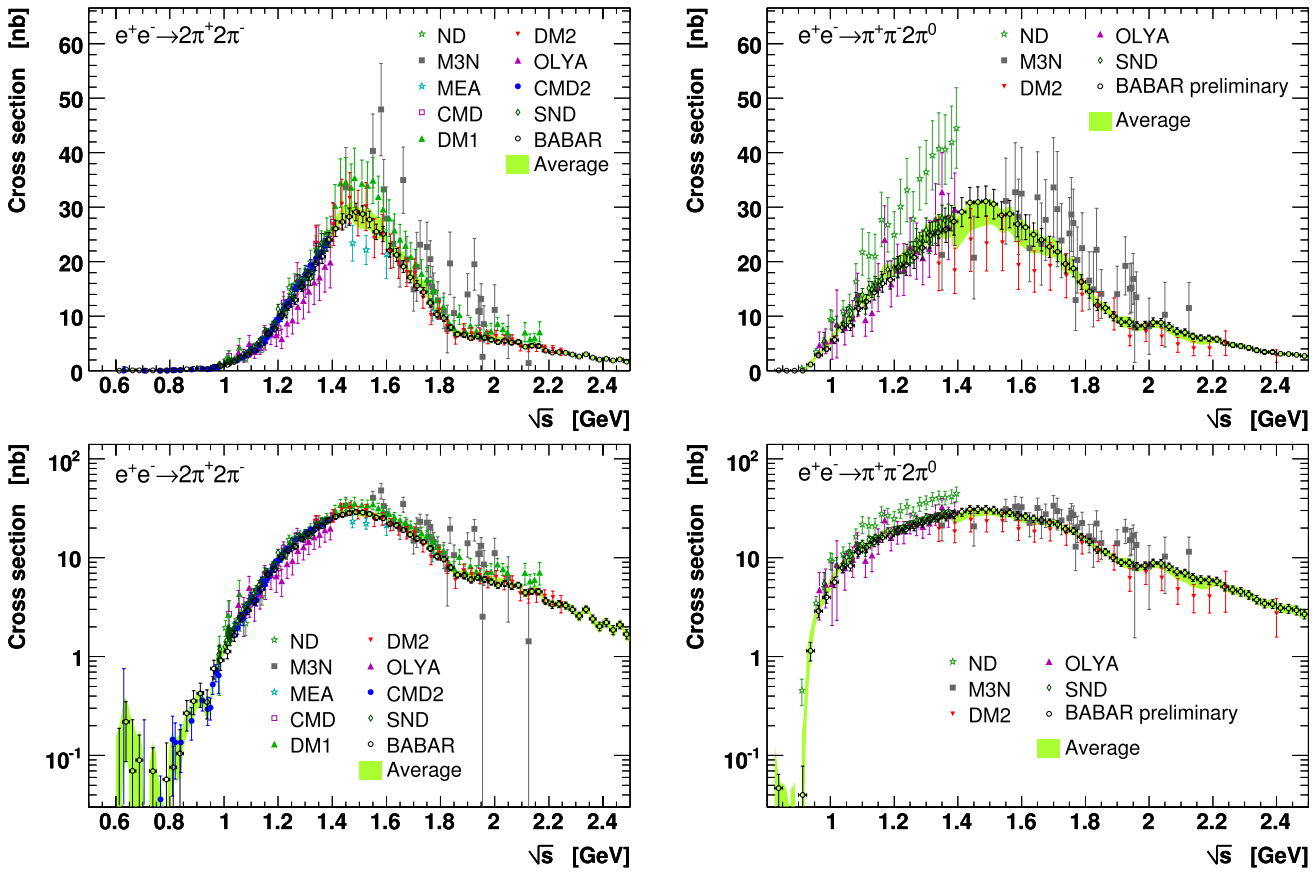

Fig. 5 Cross section versus centre-of-mass energy of $e^+e^- \to 2\pi^+2\pi^-$ (*left*) and $e^+e^- \to \pi^+\pi^-2\pi^0$ (*right*), and for linear (*top*) and logarithmic ordinates (*bottom*). The *open circles* show data from BABAR [4, 5], which dominate in precision. The other measurements shown are taken for the four charged pions final state from ND [34], M3N [35, 36], MEA [37], CMD [38], DM1 [39, 40], DM2 [41–43], OLYA [44], CMD2 [45] and SND [46, 47], and for the mixed charged and neutral state from ND [34], M3N [48, 49], DM2 [41–43], OLYA [50], and SND [46, 47]. The *error bars* show statistical and systematic errors added in quadrature. The *shaded* (*green*) *bands* give the HVPTools averages

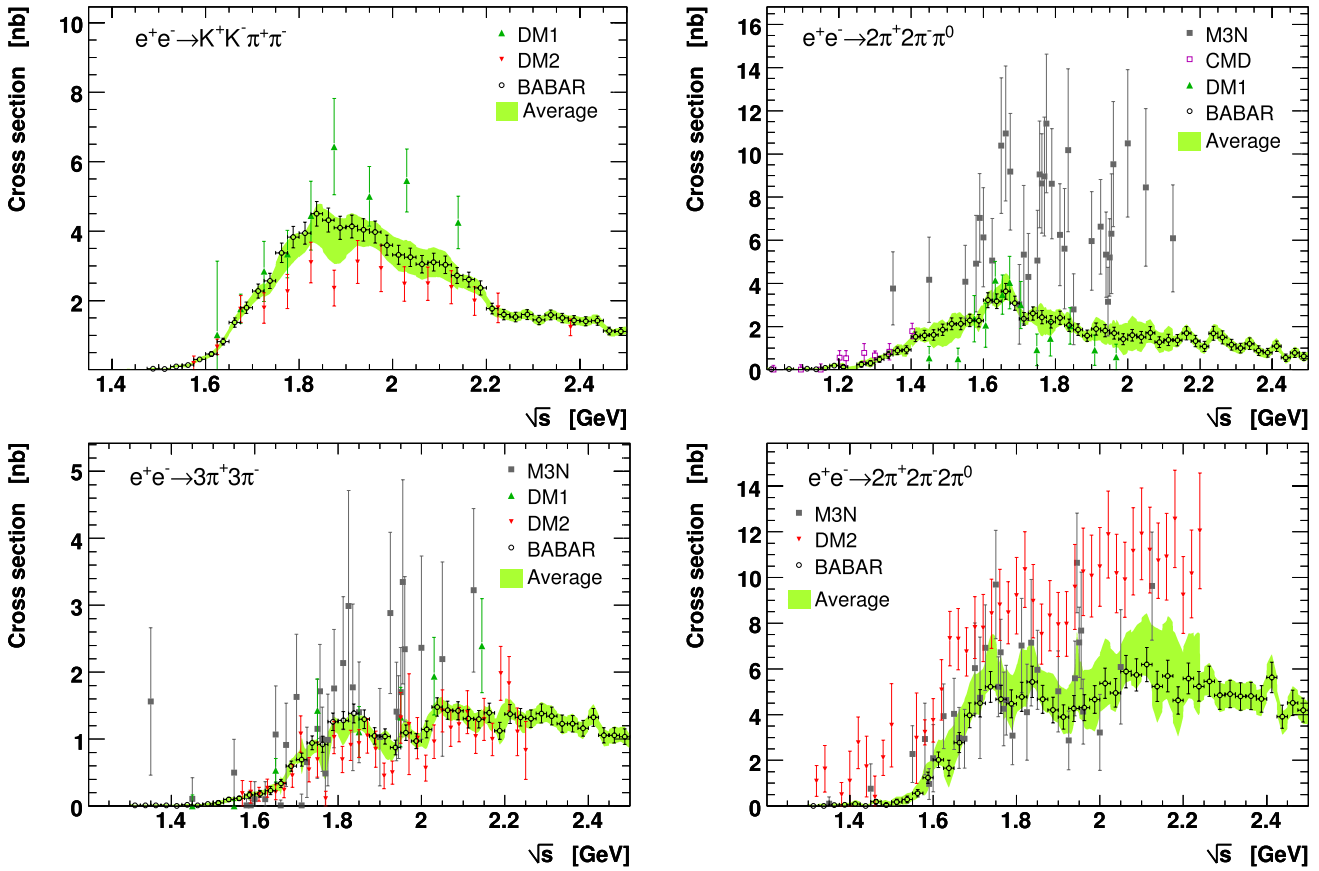

Fig. 6 Cross section data for the final states: $K^+K^-\pi^+\pi^-$ (*upper left*), $2\pi^+2\pi^-\pi^0$ (*upper right*), $3\pi^+3\pi^-$ (*lower left*) and $2\pi^+2\pi^-2\pi^0$ (*lower right*). The BABAR data points are taken from [4, 6, 7]. All the other measurements are referenced in [32, 33]. The *shaded* (*green*) *bands* give the HVPTools averages within $1\,\sigma$ errors, locally rescaled in case of incompatibilities

and HVPTools averages are depicted in Fig. 5 in linear (top) and logarithmic (bottom) ordinates.[2]

The precise BABAR data [6–9] available for several higher multiplicity modes with and without kaons (which greatly benefit from the excellent particle identification capabilities of the BABAR detector) help to discriminate between older, less precise and sometimes contradicting measurements. Figure 6 shows the cross section measurements and HVPTools averages for the channels $K^+K^-\pi^+\pi^-$ (upper left), $2\pi^+2\pi^-\pi^0$ (upper right), $3\pi^+3\pi^-$ (lower left), and $2\pi^+2\pi^-2\pi^0$ (lower right). The BABAR data supercede much less precise measurements from M3N, DM1 and DM2. In several occurrences, these older measurements overestimate the cross sections in comparison with BABAR, which contributes to the reduction in the present evaluation of the hadronic loop effects.

Finally, Fig. 7 shows the charm resonance region above the opening of the $D\overline{D}$ channel. Good agreement between the measurements is observed within the given errors. While Crystal Ball [54, 55] and BES [56–59] published bare inclusive cross section results, PLUTO applied only radiative corrections [60] following the formalism of [61], which does not include hadronic vacuum polarisation. As in previous cases [32] for the treatment of missing radiative corrections in older data, we have applied this correction and assigned a 50% systematic error to it.

3 Missing hadronic channels

Several five and six-pion modes involving π^0's, as well as $K\overline{K}[n\pi]$ final states are still unmeasured. Owing to isospin

[2] The new measurements also improve the conserved vector current (CVC) predictions for the corresponding τ decays with four pions in the final state. Coarse isospin-breaking corrections with 100% uncertainty are applied [16]. We find $\mathcal{B}_{\rm CVC}(\tau^- \to \pi^- 3\pi^0 \nu_\tau) = (1.07 \pm 0.06)\%$, to be compared to the world average of the direct measurements $(1.04 \pm 0.07)\%$ [62], and $\mathcal{B}_{\rm CVC}(\tau^- \to 2\pi^-\pi^+\pi^0\nu_\tau) = (3.79 \pm 0.21)\%$, to be compared to the direct measurement $(4.48 \pm 0.06)\%$. The deviation between prediction and measurement in the latter channel amounts to $3.2\,\sigma$, compared to $3.6\,\sigma$ without the BABAR data [32]. It is due to a discrepancy in mainly the normalisation of the corresponding τ and e^+e^- spectral functions. It is therefore important that the BABAR and Belle experiments also perform these τ branching fraction measurements as independent cross checks.

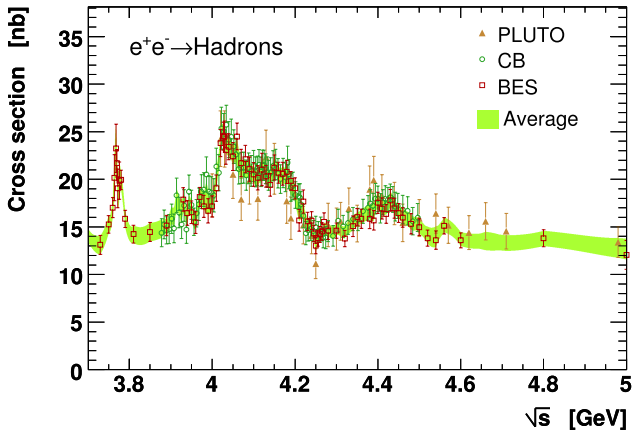

Fig. 7 Inclusive hadronic cross section versus centre-of-mass energy above the $D\overline{D}$ threshold. The measurements are taken from PLUTO [51–53], Crystal Ball [54, 55] and BES [56–59]. The *light shaded* (*green*) *band* indicates the HVPTools average within 1σ errors

invariance, their contributions can be related to those of known channels. The new BABAR cross section data and results on process dynamics thereby allow more stringent constraints of the unknown contributions than the ones obtained in our previous analyses [32, 33].

Pais isospin classes Pais introduced [63] a classification of N-pion states with total isospin $I = 0, 1$. The basis of isospin wave functions of a given state belongs to irreducible representations of the corresponding symmetry group, which are characterised by three integer quantum numbers (*partitions* of N) N_1, N_2, N_3, obeying the relations $N_1 \geq N_2 \geq N_3 \geq 0$ and $N_1 + N_2 + N_3 = N$. The total isospin I is determined uniquely to be $I = 0$ if $N_1 - N_2$ and $N_2 - N_3$ are both even, and $I = 1$ in the other cases. States $\{N_1, N_2, N_3\}$ are composed by N_3 isoscalar three-pion subsystems, $N_2 - N_3$ isovector two-pion subsystems, and $N_1 - N_2$ isovector single pions.

Simple examples are $\{110\}$ for $e^+e^- \to \pi^+\pi^-$ ($I = 1$, ρ-like), and $\{111\}$ for $e^+e^- \to \pi^+\pi^-\pi^0$ ($I = 0$, ω-like). For four pions there are two channels and two isospin classes, related at the cross section level by[3]

$$\sigma\left(e^+e^- \to 2\pi^+2\pi^-\right) = \frac{4}{5}\sigma_{310}, \tag{1}$$

$$\sigma\left(e^+e^- \to \pi^+\pi^-2\pi^0\right) = \frac{1}{5}\sigma_{310} + \sigma_{211}. \tag{2}$$

The two isospin classes correspond to the resonant final states $\rho\pi\pi$ for $\{310\}$ and $\omega\pi^0$ for $\{211\}$.

[3]In the following, and if not otherwise stated, $\sigma(X)$ denotes $\sigma(e^+e^- \to X)$.

The $I = 1$ states produced in e^+e^- are related to the vector part of specific τ decays by isospin symmetry (CVC).

Five-pion channels There are two five-pion final states, $2\pi^+2\pi^-\pi^0$ and $\pi^+\pi^-3\pi^0$, of which only the first has been measured. There is only one isospin class $\{311\}$, corresponding to $\omega\pi\pi$ and obeying the relation $\sigma(2\pi^+2\pi^-\pi^0) = 2\sigma(\pi^+\pi^-3\pi^0) = \frac{2}{3}\sigma_{311}$.

BABAR has shown [6] that the first channel is indeed dominated by $\omega\pi\pi$, with some contribution from $\eta\pi\pi$ via the isospin-violating decay $\eta \to \pi^+\pi^-\pi^0$. These η contributions must be subtracted and treated separately as they do not obey the Pais classification rules. At larger masses there is evidence for a $\rho\pi\pi$ component, which should correspond to $I_{3\pi} = 0$ contributions above the ω. Isospin symmetry holds for this contribution.

The estimation procedure for the unknown five-pion contribution is as follows: $\sigma(2\pi^+2\pi^-\pi^0)_{\eta\text{-excl}} = \sigma(2\pi^+2\pi^-\pi^0) - \sigma(\eta\pi^+\pi^-) \times \mathcal{B}(\eta \to \pi^+\pi^-\pi^0)$, with $\mathcal{B}(\eta \to \pi^+\pi^-\pi^0) = 0.2274 \pm 0.0028$ [62], $\sigma(\pi^+\pi^-3\pi^0)_{\eta\text{-excl}} = \frac{1}{2}\sigma(2\pi^+2\pi^-\pi^0)_{\eta\text{-excl}}$, and $\sigma(\eta\pi^+\pi^-)$ is considered separately. There is no contribution from $\sigma(\eta 2\pi^0)$, and the contribution of $\omega\pi\pi$ with non purely pionic ω decays is taken from $\frac{3}{2}\sigma(\omega\pi^+\pi^-) \times \mathcal{B}(\omega\text{-non-pionic})$ with $\mathcal{B}(\omega\text{-non-pionic}) = 0.093 \pm 0.007$ [62].

Six-pion channels There are three channels and four isospin classes with the relations ($I = 1$):

$$\sigma\left(3\pi^+3\pi^-\right) = \frac{24}{35}\sigma_{510} + \frac{3}{5}\sigma_{330}, \tag{3}$$

$$\sigma\left(2\pi^+2\pi^-2\pi^0\right) = \frac{8}{35}\sigma_{510} + \frac{2}{5}\sigma_{411} + \frac{2}{5}\sigma_{330} + \sigma_{321}, \tag{4}$$

$$\sigma\left(\pi^+\pi^-4\pi^0\right) = \frac{3}{35}\sigma_{510} + \frac{3}{5}\sigma_{411}, \tag{5}$$

where the lowest-mass resonant states are $\rho 4\pi$ for $\{510\}$, $\omega 3\pi$ for $\{411\}$, 3ρ for $\{330\}$, and $\omega\rho\pi$ for $\{321\}$.

BABAR has measured [7] the cross sections (3) and (4), and observed only one ρ state per event in the fully charged mode, thus favouring $\{510\}$ over $\{330\}$ in (3). The $e^+e^- \to 2\pi^+2\pi^-2\pi^0$ process is dominated by $\omega\pi^+\pi^-\pi^0$ up to 2 GeV. A small η contribution is also found, but only the cross section for $\eta\omega$ is given.

To estimate the cross section (5) the relative contributions of $\{321\}$ and $\{411\}$ need to be known, which can be constrained from τ data. The corresponding isospin relations for the τ spectral functions are

$$v\left(\tau^- \to 2\pi^+3\pi^-\pi^0\nu_\tau\right) = \frac{16}{35}v_{510} + \frac{4}{5}v_{411} + \frac{1}{5}v_{330} + \frac{1}{2}v_{321}, \tag{6}$$

$$v\left(\tau^- \to \pi^+ 2\pi^- 3\pi^0 \nu_\tau\right) = \frac{10}{35} v_{510} + \frac{1}{5} v_{411} + \frac{4}{5} v_{330} + \frac{1}{2} v_{321}, \quad (7)$$

$$v\left(\tau^- \to \pi^- 5\pi^0 \nu_\tau\right) = \frac{9}{35} v_{510}. \quad (8)$$

The branching fractions of the first two modes have been measured by CLEO. As for the e^+e^- final states, they are dominated by ω production, $\omega\pi^+2\pi^-$ and $\omega\pi^-2\pi^0$, with branching fractions $(1.20 \pm 0.22) \cdot 10^{-4}$ and $(1.4 \pm 0.5) \cdot 10^{-4}$, respectively, to be compared to total branching fractions of $(1.40 \pm 0.29) \cdot 10^{-4}$ and $(1.83 \pm 0.50) \cdot 10^{-4}$ (η subtracted). This yields the bound $v_{411}/v_{321} < 0.42$. The limit for $\pi^+\pi^-4\pi^0$ is looser than that quoted in [32], where the {411} partition was assumed to be negligible.

The estimation procedure for the missing six-pion mode is as follows: $\sigma(2\pi^+2\pi^-2\pi^0)_{\eta\text{-excl}} = \sigma(2\pi^+2\pi^-2\pi^0) - \sigma(\eta\omega) \times \mathcal{B}(\eta \to \pi^+\pi^-\pi^0) \times \mathcal{B}(\omega \to \pi^+\pi^-\pi^0)$, with $\mathcal{B}(\omega \to \pi^+\pi^-\pi^0) = 0.892 \pm 0.007$ [62], and $\sigma(\pi^+\pi^-4\pi^0) = 0.0625\sigma(3\pi^+3\pi^-) + 0.145\sigma(2\pi^+2\pi^-2\pi^0)_{\eta\text{-excl}} \pm 100\%$; $\sigma(\eta\pi^+\pi^-\pi^0) = \sigma(\eta\omega) \times \mathcal{B}(\omega \to \pi^+\pi^-\pi^0)$ is treated separately, and the contribution from non-pionic ω decays is given by $(1.145 \pm 0.145) \times \sigma(2\pi^+2\pi^-2\pi^0) \times \mathcal{B}(\omega\text{-non-pionic})/\mathcal{B}(\omega \to \pi^+\pi^-\pi^0)$.

$K\overline{K}\pi$ channels The measured final states are $K^0_S K^\pm \pi^\mp$ and $K^+K^-\pi^0$, with $K^0_S K^0_L \pi^0$ missing ($C_{K\overline{K}} = -1$). Except for a very small $\phi\pi^0$ contribution, these processes are governed by $K^0 K^{\star 0}(890)$ (dominant) and $K^\pm K^{\star\mp}(890)$ transitions below 2 GeV. Both $I = 0, 1$ amplitudes ($A_{0,1}$) contribute. The fit of the Dalitz plot in the first channel yields the moduli of the two amplitudes and their relative phase as a function of mass. Hence everything is determined, as seen from the following relations (labels written in the order $KK^\star$ with the given $K^\star$ decay modes):

$$\sigma\left(K^+K^-\pi^0 + K^-K^+\pi^0\right) = \frac{1}{6}|A_0 - A_1|^2, \quad (9)$$

$$\sigma\left(K^0_S K^0_L \pi^0 + K^0_L K^0_S \pi^0\right) = \frac{1}{6}|A_0 + A_1|^2, \quad (10)$$

$$\sigma\left(K^0 K^- \pi^+ + \overline{K}^0 K^+ \pi^-\right) = \frac{1}{3}|A_0 + A_1|^2, \quad (11)$$

$$\sigma\left(K^+ \overline{K}^0 \pi^- + K^- K^0 \pi^+\right) = \frac{1}{3}|A_0 - A_1|^2. \quad (12)$$

The measured $K^0_S K^\pm \pi^\mp$ cross section (no ordering here) is therefore equal to $\frac{1}{3}[|A_0|^2 + |A_1|^2] = \frac{1}{3}(\sigma_0 + \sigma_1)$, and $\sigma(K\overline{K}\pi) = 3\sigma(K^0_S K^\pm \pi^\mp)$ for the dominant $KK^\star$ part. Note that, unlike it was assumed in [32, 33], in general $\sigma(K^0_S K^0_L \pi^0)$ is not equal to $\sigma(K^+K^-\pi^0)$.

The complete $K\overline{K}\pi$ contribution is obtained from $\sigma(K\overline{K}\pi) = 3\sigma(K^0_S K^\pm \pi^\mp) + \sigma(\phi\pi^0) \times \mathcal{B}(\phi \to K\overline{K})$, with $\mathcal{B}(\phi \to K\overline{K}) = 0.831 \pm 0.003$, where contributions from non-hadronic ϕ decays are neglected, whereas decays to $\pi^+\pi^-\pi^0$ are already counted in the multi-pion channels.

$K\overline{K}2\pi$ channels The channels measured by BABAR are $K^+K^-\pi^+\pi^-$ and $K^+K^-2\pi^0$ [9]. They are dominated by $K^\star K\pi$, with $K\pi$ not in a $K^\star$, and smaller contributions from $K^+K^-\rho^0$ and $\phi\pi\pi$.

In the dominant $K^\star K\pi$ mode one can have $I = 0$ and $I = 1$ amplitudes. The different charge configurations can be obtained via $I_{K\pi} = 1/2$ and $3/2$ amplitudes, where, however, $I_{K\pi} = 3/2$ is not favoured because it would have predicted $\sigma(K^+K^-\pi^+\pi^-) = \sigma(K^+K^-2\pi^0)$, whereas a ratio of roughly 4:1 has been measured [9]. In the following we assume a pure $I_{K\pi} = 1/2$ state, so that the relevant cross sections read (labels in the order $K^\star K\pi$, appropriately summing over $K^0(\overline{K}^0)$)

$$\sigma\left(K^\pm\pi^0 K^\mp \pi^0\right) = \frac{1}{18}|A_0 - A_1|^2, \quad (13)$$

$$\sigma\left(K^0\pi^\pm K^\mp \pi^0\right) = \frac{1}{9}|A_0 - A_1|^2, \quad (14)$$

$$\sigma\left(K^0\pi^0 K^0 \pi^0\right) = \frac{1}{18}|A_0 + A_1|^2, \quad (15)$$

$$\sigma\left(K^\pm\pi^\mp K^0 \pi^0\right) = \frac{1}{9}|A_0 + A_1|^2, \quad (16)$$

$$\sigma\left(K^0\pi^0 K^\pm \pi^\mp\right) = \frac{1}{9}|A_0 + A_1|^2, \quad (17)$$

$$\sigma\left(K^\pm\pi^\mp K^\pm \pi^\mp\right) = \frac{2}{9}|A_0 + A_1|^2, \quad (18)$$

$$\sigma\left(K^\pm\pi^0 K^0 \pi^\mp\right) = \frac{1}{9}|A_0 - A_1|^2, \quad (19)$$

$$\sigma\left(K^0\pi^\pm K^0 \pi^\mp\right) = \frac{2}{9}|A_0 - A_1|^2. \quad (20)$$

This leads to $\sigma(K\overline{K}\pi\pi) = 9\sigma(K^+K^-\pi^0\pi^0) + \frac{9}{4}\sigma \times (K^+K^-\pi^+\pi^-)$.

The inclusive $\sigma(K\overline{K}\rho)$ cross section is thus obtained as follows: get $\sigma(\phi\pi^+\pi^-) = 2\sigma(\phi 2\pi^0)$ and $\sigma(K^+K^-\rho^0) = \sigma(K^+K^-\pi^+\pi^-) - \sigma(K^{\star 0}K^\pm\pi^\mp) - \sigma(\phi\pi^+\pi^-) \times \mathcal{B}(\phi \to K^+K^-)$ (note that the published BABAR cross section table for $K^{\star 0}K^\pm\pi^\mp$ already includes the branching fraction for $K^{\star 0} \to K^\pm\pi^\mp$). In lack of more information, we assume $\sigma(K\overline{K}\rho) = 4\sigma(K^+K^-\rho^0)$, with a 100% error, and obtain $\sigma(K\overline{K}\pi\pi) = 9[\sigma(K^+K^-2\pi^0) - \sigma(\phi 2\pi^0)] + \frac{9}{4}\sigma(K^{\star 0}K^\pm\pi^\mp) + \frac{3}{2}\sigma(\phi\pi^+\pi^-) + 4\sigma(K^+K^-\rho^0)$.

$K\overline{K}3\pi$ channels BABAR has only measured the final state $K^+K^-\pi^+\pi^-\pi^0$ [6], which is dominated by $K^+K^-\omega$ up to 2 GeV. The channel $\phi\eta$ has been measured, and the remaining $\phi\pi^+\pi^-\pi^0$ amplitude is negligible. The ω dominance does not apply to the missing channels

$K^0K^\pm\pi^\mp\pi^+\pi^-$ and $K^0K^\pm\pi^\mp 2\pi^0$, but their dynamics (for instance $K^\star$) should be seen in the measured $K^+K^-\pi^+\pi^-\pi^0$ mode, so it may be small, at least below 2 GeV.

The missing channels are estimated as follows: $\sigma(K^+K^-\pi^+\pi^-\pi^0)_{\eta\text{-excl}} =! \sigma(K^+K^-\pi^+\pi^-\pi^0) - \sigma(\phi\eta) \times \mathcal{B}(\phi \to K^+K^-) \times \mathcal{B}(\eta \to \pi^+\pi^-\pi^0)$. We assume, within a systematic error of 50%, $\sigma(K^0\overline{K}^0\pi^+\pi^-\pi^0)_{\eta\text{-excl}} = \sigma(K^+K^-\pi^+\pi^-\pi^0)_{\eta\text{-excl}}$, treat $\sigma(\phi\eta)$ separately, and compute the non-pionic ω contribution by $2\sigma(K^+K^-\pi^+\pi^-\pi^0)_{\eta\text{-excl}} \times \mathcal{B}(\omega\text{-non-pionic})/\mathcal{B}(\omega \to \pi^+\pi^-\pi^0)$. Contributions from $K^0K^\pm\pi^\mp\pi^+\pi^-$ and $K^0K^\pm\pi^\mp 2\pi^0$ below 2 GeV are neglected.

$\eta 4\pi$ channels BABAR has measured $\sigma(\eta 2\pi^+2\pi^-)$ [6], where the 4π state has $C=-1$, $I=1$. Because $\sigma(2\pi^+2\pi^-) \approx \sigma(\pi^+\pi^-2\pi^0)$, we assume the same ratio for the $\eta 4\pi$ process with the same 4π quantum numbers. We thus estimate $\sigma(\eta 4\pi) = 2\sigma(\eta 2\pi^+2\pi^-)$, and assign a systematic error of 25% to it.

4 Data averaging and integration

In this work, we have extended the use of HVPTools[4] to all experimental cross section data used in the compilation.[5] The main difference of HVPTools with respect to our earlier software is that it replaces linear interpolation between adjacent data points ("trapezoidal rule") by quadratic interpolation, which is found from toy-model analyses, with known truth integrals, to be more accurate. The interpolation functions are locally averaged between experiments, whereby correlations between measurement points of the same experiment and among different experiments due to common systematic errors are fully taken into account. Incompatible measurements lead to error rescaling in the local averages, using the PDG prescription [62].

The errors in the average and in the integration for each channel are obtained from large samples of pseudo Monte Carlo experiments, by fluctuating all data points within errors and along their correlations. The integrals of the exclusive channels are then summed up, and the error of the sum is obtained by adding quadratically (linearly) all uncorrelated (correlated) errors.

Common sources of systematic errors also occur between measurements of different final state channels and must be taken into account when summing up the exclusive contributions. Such correlations mostly arise from luminosity uncertainties, if the data stem from the same experimental facility, and from radiative corrections. In total eight categories of correlated systematic uncertainties are distinguished. Among those the most significant belong to radiative corrections, which are the same for CMD2 and SND, as well as to luminosity determinations by BABAR, CMD2 and SND (correlated per experiment for different channels, but independent between different experiments).

5 Results

A compilation of all contributions to $a_\mu^{\text{had,LO}}$ and to $\Delta\alpha_{\text{had}}(M_Z^2)$, as well as the total results, are given in Table 2. The experimental errors are separated into statistical, channel-specific systematic, and common systematic contributions that are correlated with at least one other channel.

Table 1 quotes the specific contributions of the various $e^+e^- \to \pi^+\pi^-$ cross section measurements to $a_\mu^{\text{had,LO}}$. Also given are the corresponding CVC-based $\tau \to \pi^-\pi^0\nu_\tau$ branching fraction predictions. The largest (smallest) discrepancy of 2.7σ (1.2σ) between prediction and direct measurement is exhibited by KLOE (BABAR). It is interesting to note that the four $a_\mu^{\text{had,LO}}[\pi^+\pi^-]$ determinations in Table 1 agree within errors (the overall χ^2 of their average amounts to 3.2 for 3 degrees of freedom), whereas significant discrepancies are observed in the corresponding spectral functions [10]. Since we cannot think of good reasons why systematic effects affecting the spectral functions should necessarily cancel in the integrals, we refrain from averaging the four values with a resulting smaller error. The combined contribution is instead computed from local averages of the spectral function data that are subjected to local error rescaling in case of incompatibilities.

The contributions of the J/ψ and $\psi(2S)$ resonances in Table 2 are obtained by numerically integrating the cor-

Table 1 Contributions to $a_\mu^{\text{had,LO}}$ (middle column) from the individual $\pi^+\pi^-$ cross section measurements by BABAR [2], KLOE [1, 13], CMD2 [20–23], and SND [24]. Also given are the corresponding CVC predictions of the $\tau \to \pi^-\pi^0\nu_\tau$ branching fraction (right column), corrected for isospin-breaking effects [15]. Here the first error is experimental and the second estimates the uncertainty in the isospin-breaking corrections. The predictions are to be compared with the world average of the direct branching fraction measurements $(25.51 \pm 0.09)\%$ [62]. For each experiment, all available data in the energy range from threshold to 1.8 GeV (m_τ for $\mathcal{B}_{\text{CVC}}$) are used, and the missing part is completed by the combined e^+e^- data. The corresponding (integrand dependent) fractions of the full integrals provided by a given experiment are given in parentheses

Experiment	$a_\mu^{\text{had,LO}}$ $[10^{-10}]$	$\mathcal{B}_{\text{CVC}}$ [%]
BABAR	514.1 ± 3.8 (1.00)	$25.15 \pm 0.18 \pm 0.22$ (1.00)
KLOE	503.1 ± 7.1 (0.97)	$24.56 \pm 0.26 \pm 0.22$ (0.92)
CMD2	506.6 ± 3.9 (0.89)	$24.96 \pm 0.21 \pm 0.22$ (0.96)
SND	505.1 ± 6.7 (0.94)	$24.82 \pm 0.30 \pm 0.22$ (0.91)

[4] See [10] for a more detailed description of the averaging and integration procedure developed for HVPTools.

[5] So far [10], only the two-pion and four-pion channels were fully evaluated using HVPTools, while all other contributions were taken from our previous publications, using less sophisticated averaging software.

Table 2 Compilation of the exclusive and inclusive contributions to $a_\mu^{\mathrm{had,LO}}$ and $\Delta\alpha_{\mathrm{had}}(M_Z^2)$. Where three (or more) errors are given, the first is statistical, the second channel-specific systematic, and the third common systematic, which is correlated with at least one other channel. For the contributions computed from QCD, only total errors are given, which include effects from the α_S uncertainty, the truncation of the perturbative series at four loops, the FOPT vs. CIPT ambiguity (see text), and quark mass uncertainties. Apart from the latter uncertainty, all other errors are taken to be fully correlated among the various energy regions where QCD is used. The errors in the Breit–Wigner integrals of the narrow resonances J/ψ and $\psi(2S)$ are dominated by the uncertainties in their respective electronic width measurements [62]. The error on the sum (last line) is obtained by quadratically adding all statistical and channel-specific systematic errors, and by linearly adding correlated systematic errors where applies (see text for details on the treatment of correlations between different channels)

Channel	$a_\mu^{\mathrm{had,LO}}$ $[10^{-10}]$	$\Delta\alpha_{\mathrm{had}}(M_Z^2)$ $[10^{-4}]$
$\pi^0\gamma$	$4.42 \pm 0.08 \pm 0.13 \pm 0.12$	$0.36 \pm 0.01 \pm 0.01 \pm 0.01$
$\eta\gamma$	$0.64 \pm 0.02 \pm 0.01 \pm 0.01$	$0.08 \pm 0.00 \pm 0.00 \pm 0.00$
$\pi^+\pi^-$	$507.80 \pm 1.22 \pm 2.50 \pm 0.56$	$34.43 \pm 0.07 \pm 0.17 \pm 0.04$
$\pi^+\pi^-\pi^0$	$46.00 \pm 0.42 \pm 1.03 \pm 0.98$	$4.58 \pm 0.04 \pm 0.11 \pm 0.09$
$2\pi^+2\pi^-$	$13.35 \pm 0.10 \pm 0.43 \pm 0.29$	$3.49 \pm 0.03 \pm 0.12 \pm 0.08$
$\pi^+\pi^-2\pi^0$	$18.01 \pm 0.14 \pm 1.17 \pm 0.40$	$4.43 \pm 0.03 \pm 0.29 \pm 0.10$
$2\pi^+2\pi^-\pi^0$ (η excl.)	$0.72 \pm 0.04 \pm 0.07 \pm 0.03$	$0.22 \pm 0.01 \pm 0.02 \pm 0.01$
$\pi^+\pi^-3\pi^0$ (η excl., from isospin)	$0.36 \pm 0.02 \pm 0.03 \pm 0.01$	$0.11 \pm 0.01 \pm 0.01 \pm 0.00$
$3\pi^+3\pi^-$	$0.12 \pm 0.01 \pm 0.01 \pm 0.00$	$0.04 \pm 0.00 \pm 0.00 \pm 0.00$
$2\pi^+2\pi^-2\pi^0$ (η excl.)	$0.70 \pm 0.05 \pm 0.04 \pm 0.09$	$0.25 \pm 0.02 \pm 0.02 \pm 0.03$
$\pi^+\pi^-4\pi^0$ (η excl., from isospin)	$0.11 \pm 0.01 \pm 0.11 \pm 0.00$	$0.04 \pm 0.00 \pm 0.04 \pm 0.00$
$\eta\pi^+\pi^-$	$1.15 \pm 0.06 \pm 0.08 \pm 0.03$	$0.33 \pm 0.02 \pm 0.02 \pm 0.01$
$\eta\omega$	$0.47 \pm 0.04 \pm 0.00 \pm 0.05$	$0.15 \pm 0.01 \pm 0.00 \pm 0.02$
$\eta 2\pi^+2\pi^-$	$0.02 \pm 0.01 \pm 0.00 \pm 0.00$	$0.01 \pm 0.00 \pm 0.00 \pm 0.00$
$\eta\pi^+\pi^-2\pi^0$ (estimated)	$0.02 \pm 0.01 \pm 0.01 \pm 0.00$	$0.01 \pm 0.00 \pm 0.00 \pm 0.00$
$\omega\pi^0$ ($\omega \to \pi^0\gamma$)	$0.89 \pm 0.02 \pm 0.06 \pm 0.02$	$0.18 \pm 0.00 \pm 0.02 \pm 0.00$
$\omega\pi^+\pi^-, \omega 2\pi^0$ ($\omega \to \pi^0\gamma$)	$0.08 \pm 0.00 \pm 0.01 \pm 0.00$	$0.03 \pm 0.00 \pm 0.00 \pm 0.00$
ω (non-$3\pi, \pi\gamma, \eta\gamma$)	$0.36 \pm 0.00 \pm 0.01 \pm 0.00$	$0.03 \pm 0.00 \pm 0.00 \pm 0.00$
K^+K^-	$21.63 \pm 0.27 \pm 0.58 \pm 0.36$	$3.13 \pm 0.04 \pm 0.08 \pm 0.05$
$K_S^0K_L^0$	$12.96 \pm 0.18 \pm 0.25 \pm 0.24$	$1.75 \pm 0.02 \pm 0.03 \pm 0.03$
ϕ (non-$K\overline{K}, 3\pi, \pi\gamma, \eta\gamma$)	$0.05 \pm 0.00 \pm 0.00 \pm 0.00$	$0.01 \pm 0.00 \pm 0.00 \pm 0.00$
$K\overline{K}\pi$ (partly from isospin)	$2.39 \pm 0.07 \pm 0.12 \pm 0.08$	$0.00 \pm 0.02 \pm 0.04 \pm 0.02$
$K\overline{K}2\pi$ (partly from isospin)	$1.35 \pm 0.09 \pm 0.38 \pm 0.03$	$0.48 \pm 0.03 \pm 0.14 \pm 0.01$
$K\overline{K}3\pi$ (partly from isospin)	$-0.03 \pm 0.01 \pm 0.02 \pm 0.00$	$-0.01 \pm 0.00 \pm 0.01 \pm 0.00$
$\phi\eta$	$0.36 \pm 0.02 \pm 0.02 \pm 0.01$	$0.13 \pm 0.01 \pm 0.01 \pm 0.00$
$\omega K\overline{K}$ ($\omega \to \pi^0\gamma$)	$0.00 \pm 0.00 \pm 0.00 \pm 0.00$	$0.00 \pm 0.00 \pm 0.00 \pm 0.00$
J/ψ (Breit–Wigner integral)	6.22 ± 0.16	7.03 ± 0.18
$\psi(2S)$ (Breit–Wigner integral)	1.57 ± 0.03	2.50 ± 0.04
R_{data} [3.7–5.0 GeV]	$7.29 \pm 0.05 \pm 0.30 \pm 0.00$	$15.79 \pm 0.12 \pm 0.66 \pm 0.00$
R_{QCD} [1.8–3.7 GeV]$_{uds}$	33.45 ± 0.28	24.27 ± 0.19
R_{QCD} [5.0–9.3 GeV]$_{udsc}$	6.86 ± 0.04	34.89 ± 0.18
R_{QCD} [9.3–12.0 GeV]$_{udscb}$	1.21 ± 0.01	15.56 ± 0.04
R_{QCD} [12.0–40.0 GeV]$_{udscb}$	1.64 ± 0.01	77.94 ± 0.12
R_{QCD} [> 40.0 GeV]$_{udscb}$	0.16 ± 0.00	42.70 ± 0.06
R_{QCD} [> 40.0 GeV]$_t$	0.00 ± 0.00	-0.72 ± 0.01
Sum	$692.3 \pm 1.4 \pm 3.1 \pm 2.4$ $\pm 0.2_\psi \pm 0.3_{\mathrm{QCD}}$	$274.21 \pm 0.17 \pm 0.78 \pm 0.37$ $\pm 0.18_\psi \pm 0.52_{\mathrm{QCD}}$

responding undressed[6] Breit–Wigner lineshapes. Using instead the narrow-width approximation, $\sigma_R = 12\pi^2\Gamma^0_{ee}/M_R \cdot \delta(s - M_R^2)$, gives compatible results. The errors in the integrals are dominated by the knowledge of the corresponding bare electronic width $\Gamma^0_{R\to ee}$.

Sufficiently far from the quark thresholds we use four-loop [11] perturbative QCD, including $\mathcal{O}(\alpha_s^2)$ quark mass corrections [64], to compute the inclusive hadronic cross section. Non-perturbative contributions at 1.8 GeV were determined from data [65] and found to be small. The errors of the $R_{\rm QCD}$ contributions given in Table 2 account for the uncertainty in α_s (we use $\alpha_s(M_Z^2) = 0.1193 \pm 0.0028$ from the fit to the Z hadronic width [66]), the truncation of the perturbative series (we use the full four-loop contribution as systematic error), the full difference between fixed-order perturbation theory (FOPT) and, so-called, contour-improved perturbation theory (CIPT) [67], as well as quark mass uncertainties (we use the values and errors from [62]). The former three errors are taken to be fully correlated between the various energy regions (see Table 2), whereas the (smaller) quark-mass uncertainties are taken to be uncorrelated. Figure 8 shows the comparison between BES data [56–59] and the QCD prediction below the $D\overline{D}$ threshold between 2 and 3.7 GeV. Agreement within errors is found.[7]

Muon magnetic anomaly Adding all lowest-order hadronic contributions together yields the estimate (this and all following numbers in this and the next paragraph are in units of 10^{-10})

$$a_\mu^{\rm had,LO} = 692.3 \pm 4.2 \tag{21}$$

which is dominated by experimental systematic uncertainties (cf. Table 2 for a separation of the error into subcomponents). The new result is $-3.2 \cdot 10^{-10}$ below that of our previous evaluation [10]. This shift is composed of -0.7 from the inclusion of the new, large photon angle data from KLOE, $+0.4$ from the use of preliminary BABAR data in the $e^+e^- \to \pi^+\pi^-2\pi^0$ mode, -2.4 from the new high-multiplicity exclusive channels, the reestimate of the unknown channels, and the new resonance treatment, -0.5 from mainly the four-loop term in the QCD prediction of the hadronic cross section that contributes with a negative sign, as well as smaller other differences. The total error on $a_\mu^{\rm had,LO}$ is slightly larger than that of [10] owing to a more thorough (and conservative) evaluation of the inter-channel correlations.

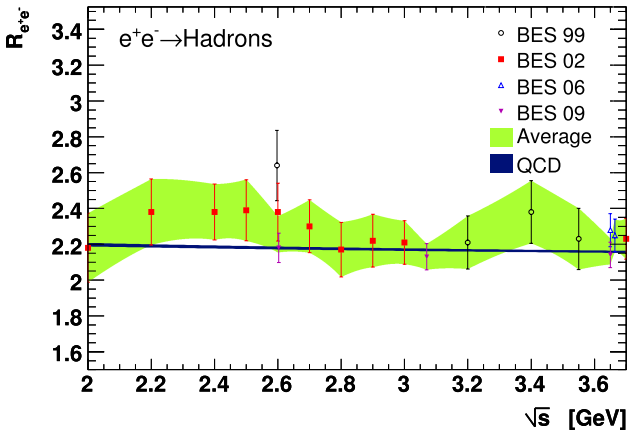

Fig. 8 Inclusive hadronic cross section ratio versus centre-of-mass energy in the continuum region below the $D\overline{D}$ threshold. Shown are bare BES data points [56–59], with statistical and systematic errors added in quadrature, the data average (*shaded band*), and the prediction from massive perturbative QCD (solid line—see text)

Adding to the result (21) the contributions from higher order hadronic loops, -9.79 ± 0.09 [70], hadronic light-by-light scattering, 10.5 ± 2.6 [72] (cf. remark in Footnote 8), as well as QED, $11\,658\,471.809 \pm 0.015$ [73] (see also [68] and references therein), and electroweak effects, $15.4 \pm 0.1_{\rm had} \pm 0.2_{\rm Higgs}$ [74–76], we obtain the SM prediction

$$a_\mu^{\rm SM} = 11\,659\,180.2 \pm 4.2 \pm 2.6 \pm 0.2\ (4.9_{\rm tot}), \tag{22}$$

where the errors account for lowest and higher order hadronic, and other contributions, respectively. The result (22) deviates from the experimental average, $a_\mu^{\rm exp} = 11\,659\,208.9 \pm 5.4 \pm 3.3$ [12, 68], by 28.7 ± 8.0 (3.6σ).[8]

A compilation of recent SM predictions for a_μ compared with the experimental result is given in Fig. 9.

Update of τ-based $g-2$ result The majority of the changes applied in this work, compared to our previous one [10], will similarly affect the τ-based result from [15], requiring a reevaluation of the corresponding τ-based hadronic contribution. In the τ-based analysis [78], the $\pi^+\pi^-$ cross section is entirely replaced by the average, isospin-transformed, and isospin-breaking corrected

[6] The undressing uses the BABAR programme *Afkvac* correcting for both leptonic and hadronic vacuum polarisation effects. The correction factors amount to $(1 - \Pi(s))^2 = 0.956$ and 0.957 for the J/ψ and $\psi(2S)$, respectively.

[7] To study the transition region between the sum of exclusive measurements and QCD, we have computed $a_\mu^{\rm had,LO}$ in two narrow energy intervals around 1.8 GeV. For the energy interval 1.75–1.8 GeV we find (in units of 10^{-10}) $2.74 \pm 0.06 \pm 0.21$ (statistical and systematic errors) for the sum of the exclusive data, and 2.53 ± 0.03 for perturbative QCD (see text for the contributions to the error). For the interval 1.8–2.0 GeV we find $8.28 \pm 0.11 \pm 0.74$ and 8.31 ± 0.09 for data and QCD, respectively. The excellent agreement represents another support for the use of QCD beyond 1.8 GeV centre-of-mass energy. Comparing the $a_\mu^{\rm had,LO}$ predictions in the energy interval 2–3.7 GeV, we find $26.5 \pm 0.2 \pm 1.7$ for BES data, and 25.2 ± 0.2 for perturbative QCD.

[8] Using the alternative result for the light-by-light scattering contribution, 11.6 ± 4.0 [77], the error in the SM prediction (22) increases to 5.8, and the discrepancy with experiment reduces to 3.2σ.

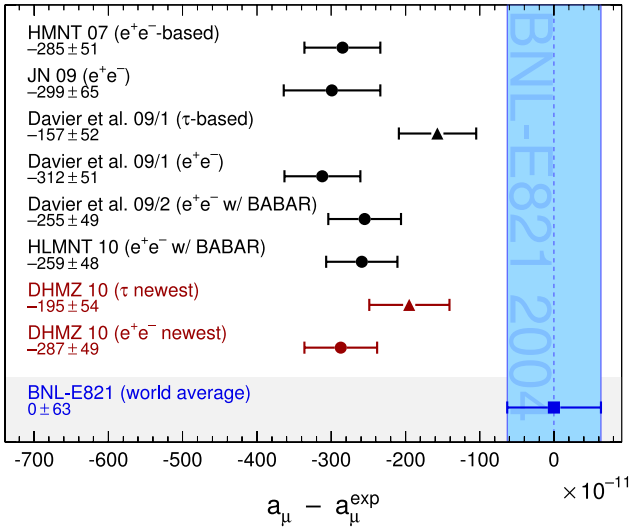

Fig. 9 Compilation of recent results for a_μ^{SM} (in units of 10^{-11}), subtracted by the central value of the experimental average [12, 68]. The *shaded vertical band* indicates the experimental error. The SM predictions are taken from: this work (DHMZ 10), HLMNT (unpublished) [69] (e^+e^- based, including BABAR and KLOE 2010 $\pi^+\pi^-$ data), Davier et al. 09/1 [15] (τ-based), Davier et al. 09/1 [15] (e^+e^--based, not including BABAR $\pi^+\pi^-$ data), Davier et al. 09/2 [10] (e^+e^--based including BABAR $\pi^+\pi^-$ data), HMNT 07 [70] and JN 09 [71] (not including BABAR $\pi^+\pi^-$ data)

$\tau \to \pi^-\pi^0\nu_\tau$ spectral function,[9] while the four-pion cross sections, obtained from linear combinations of the $\tau^- \to \pi^-3\pi^0\nu_\tau$ and $\tau^- \to 2\pi^-\pi^+\pi^0\nu_\tau$ spectral functions,[10] are only evaluated up to 1.5 GeV with τ data. Due to the lack of statistical precision, the spectrum is completed with e^+e^- data between 1.5 and 1.8 GeV. All the other channels are taken from e^+e^- data. The complete lowest-order τ-based result reads

$$a_\mu^{\mathrm{had,LO}}[\tau] = 701.5 \pm 3.5 \pm 1.9 \pm 2.4 \pm 0.2 \pm 0.3, \qquad (23)$$

where the first error is τ experimental, the second estimates the uncertainty in the isospin-breaking corrections, the third is e^+e^- experimental, and the fourth and fifth stand for the narrow resonance and QCD uncertainties, respectively. The τ-based hadronic contribution deviates by 9.1 ± 5.0 ($1.8\,\sigma$) from the e^+e^--based one, and the full τ-based SM prediction $a_\mu^{\mathrm{SM}}[\tau] = 11\,659\,189.4 \pm 5.4$ deviates by 19.5 ± 8.3 ($2.4\,\sigma$) from the experimental average. The new τ-based result is also included in the compilation of Fig. 9.

[9]Using published $\tau \to \pi^-\pi^0\nu_\tau$ spectral function data from ALEPH [79], Belle [80], CLEO [81] and OPAL [82], and using the world average branching fraction [62] (2009 PDG edition).

[10]Similar to Footnote 2, coarse isospin-breaking corrections with 100% uncertainty are applied to the four-pion spectral functions from τ decays [16].

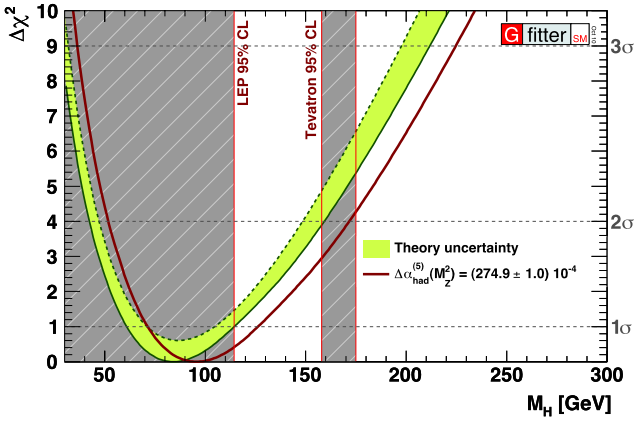

Fig. 10 Standard Gfitter electroweak fit result [66] (*light shaded band*) and the result obtained for the new evaluation of $\Delta\alpha_{\mathrm{had}}(M_Z^2)$ (*solid* (*red*) *curve*). The legend displays the corresponding five-quark contribution, $\Delta\alpha_{\mathrm{had}}^{(5)}(M_Z^2)$, where the top term of $-0.72 \cdot 10^{-4}$ is excluded. A shift of +12 GeV in the central value of the Higgs boson is observed

Running electromagnetic coupling at M_Z^2 The sum of all hadronic contributions from Table 2 gives for the e^+e^--based hadronic term in the running of $\alpha(M_Z^2)$

$$\Delta\alpha_{\mathrm{had}}(M_Z^2) = (274.2 \pm 1.0) \cdot 10^{-4}, \qquad (24)$$

which is, contrary to the evaluation of $a_\mu^{\mathrm{had,LO}}$, not dominated by the uncertainty in the experimental low-energy data, but by contributions from all energy regions, where both experimental and theoretical errors have similar magnitude.[11] The corresponding τ-based result reads $\Delta\alpha_{\mathrm{had}}(M_Z^2) = (275.4 \pm 1.1) \cdot 10^{-4}$. As expected, the result (24) is smaller than the most recent (unpublished) value from the HLMNT group [69] $\Delta\alpha_{\mathrm{had}}(M_Z^2) = (275.2 \pm 1.5) \cdot 10^{-4}$. Owing to the use of perturbative QCD between 1.8 and 3.7 GeV, the precision in (24) is significantly improved compared to the HLMNT result, which relies on experimental data in that domain.[12]

Adding the three-loop leptonic contribution, $\Delta\alpha_{\mathrm{lep}}(M_Z^2) = 314.97686 \cdot 10^{-4}$ [83], with negligible uncertainties, one finds

$$\alpha^{-1}\left(M_Z^2\right) = 128.962 \pm 0.014. \qquad (25)$$

The running electromagnetic coupling at M_Z enters at various levels the global SM fit to electroweak precision

[11]In the global electroweak fit both $\alpha_s(M_Z)$ and $\Delta\alpha_{\mathrm{had}}(M_Z^2)$ are floating parameters (though the latter one is constrained to its phenomenological value). It is therefore important to include their mutual dependence in the fit. The functional dependence of the central value of $\Delta\alpha_{\mathrm{had}}(M_Z^2)$ on the value of $\alpha_s(M_Z^2)$ approximately reads $0.37 \cdot 10^{-4} \times (\alpha_s(M_Z^2) - 0.1193)/0.0028$.

[12]HLMNT use perturbative QCD for the central value of the contribution between 1.8 and 3.7 GeV, but assign the experimental errors from the BES measurements to it.

data. It contributes to the radiator functions that modify the vector and axial-vector couplings in the partial Z boson widths to fermions, and also to the SM prediction of the W mass and the effective weak mixing angle. Overall, the fit exhibits a -39% correlation between the Higgs mass (M_H) and $\Delta\alpha_{\rm had}(M_Z^2)$ [66], so that the decrease in the value (24) and thus in the running electromagnetic coupling strength, with respect to earlier evaluations, leads to an increase in the most probable value of M_H returned by the fit.[13] Figure 10 shows the standard Gfitter result (light shaded band) [66], using as hadronic contribution $\Delta\alpha_{\rm had}(M_Z^2) = (276.8 \pm 2.2) \cdot 10^{-4}$ [70], together with the result obtained by using (24) (solid line). The fitted Higgs mass shifts from previously 84^{+30}_{-23} GeV to 96^{+31}_{-24} GeV. The larger error of the latter value, in spite of the improved accuracy in $\Delta\alpha_{\rm had}(M_Z^2)$, is due to the logarithmic M_H dependence of the fit observables. The new 95% and 99% upper limits on M_H are 170 GeV and 201 GeV, respectively.

6 Conclusions

We have updated the Standard Model predictions of the muon anomalous magnetic moment and the running electromagnetic coupling constant at M_Z^2 by reevaluating their virtual hadronic contributions. Mainly the reestimation of missing higher multiplicity channels, owing to new results from BABAR, causes a decrease of this contribution with respect to earlier calculations, which—on one hand—amplifies the discrepancy of the muon $g-2$ measurement with its prediction to $3.6\,\sigma$ for e^+e^--based analysis, and to $2.4\,\sigma$ for the τ-based analysis, while—on the other hand—relaxes the tension between the direct Higgs searches and the electroweak fit by 12 GeV for the Higgs mass.

A thorough reestimation of inter-channel correlations has led to a slight increase in the final error of the hadronic contribution to the muon $g-2$. A better precision is currently constricted by the discrepancy between KLOE and the other experiments, in particular BABAR, in the dominant $\pi^+\pi^-$ mode. This discrepancy is corroborated when comparing e^+e^- and τ data in this mode, where agreement between BABAR and τ data is observed.

Support for the KLOE results must come from a cross-section measurement involving the ratio of pion-to-muon pairs. Moreover, new $\pi^+\pi^-$ precision data are soon expected from the upgraded VEPP-2000 storage ring at BINP-Novosibirsk, Russia, and the improved detectors CMD-3 and SND-2000. The future development of this field also relies on a more accurate muon $g-2$ measurement, and on progress in the evaluation of the light-by-light scattering contribution.

[13] The correlation between M_H and $\Delta\alpha_{\rm had}(M_Z^2)$ reduces to -17% when using the result (24) in the global fit.

Acknowledgements We are most grateful to Martin Goebel from the Gfitter group for performing the electroweak fit and producing Fig. 10 of this paper. We thank Changzheng Yuan, Andreas Bäcker and Claus Grupen for information on the radiative corrections applied to BES and PLUTO data. This work is supported in part by the Talent Team Program of CAS (KJCX2-YW-N45) of China.

References

1. F. Ambrosino et al. (KLOE Collaboration) (2010). arXiv:1006.5313
2. B. Aubert et al. (BABAR Collaboration), Phys. Rev. Lett. **103**, 231801 (2009). arxiv:0908.3589
3. B. Aubert et al. (BABAR Collaboration), Phys. Rev. D **70**, 072004 (2004). hep-ex/0408078
4. B. Aubert et al. (BABAR Collaboration), Phys. Rev. D **71**, 052001 (2005). hep-ex/0502025
5. V.P. Druzhinin, Study of e^+e^- annihilation at low energies. Presented at 23rd International Symposium on Lepton-Photon Interactions at High Energy (LP07), Daegu, Korea, 13–18 Aug 2007, published in Daegu 2007, Lepton and Photon Interactions at High Energies 134. arXiv:0710.3455
6. B. Aubert et al. (BABAR Collaboration), Phys. Rev. D **76**, 092005 (2007). Erratum-ibid. D **77**, 119902 (2008). arXiv:0708.2461
7. B. Aubert et al. (BABAR Collaboration), Phys. Rev. D **73**, 052003 (2006). hep-ex/0602006
8. B. Aubert et al. (BABAR Collaboration), Phys. Rev. D **77**, 092002 (2008). arXiv:0710.4451
9. B. Aubert et al. (BABAR Collaboration), Phys. Rev. D **76**, 012008 (2007). arXiv:0704.0630
10. M. Davier, A. Hoecker, B. Malaescu, C.Z. Yuan, Z. Zhang, Eur. Phys. J. C **66**, 1 (2010). arXiv:0908.4300
11. P. Baikov, K.G. Chetyrkin, J.H. Kühn, Phys. Rev. Lett. **101**, 012002 (2008). arXiv:0801.1821
12. G.W. Bennett et al. (Muon $g-2$ Collaboration), Phys. Rev. D **73**, 072003 (2006). hep-ex/0602035
13. F. Ambrosino et al. (KLOE Collaboration), Phys. Lett. B **670**, 285 (2009). arXiv:0809.3950
14. F. Aloisio et al. (KLOE Collaboration), Phys. Lett. B **606**, 12 (2005). hep-ex/0407048
15. M. Davier et al. Eur. Phys. J. C **66**, 127 (2010). arXiv:0906.5443
16. H. Czyz, J.H. Kühn, Eur. Phys. J. C **18**, 497 (2001). hep-ph/0008262
17. I.B. Vasserman et al. (TOF Collaboration), Sov. J. Nucl. Phys. **33**, 368 (1981)
18. L.M. Barkov et al. (OLYA, CMD Collaborations), Nucl. Phys. B **256**, 365 (1985)
19. I.B. Vasserman et al. (OLYA Collaboration), Sov. J. Nucl. Phys. **30**, 519 (1979)
20. R.R. Akhmetshin et al. (CMD2 Collaboration), Phys. Lett. B **578**, 285 (2004). hep-ex/0308008
21. V.M. Aulchenko et al. (CMD2 Collaboration), JETP Lett. **82**, 743 (2005). hep-ex/0603021
22. R.R. Akhmetshin et al. (CMD2 Collaboration), JETP Lett. **84**, 413 (2006). hep-ex/0610016
23. R.R. Akhmetshin et al. (CMD2 Collaboration), Phys. Lett. B **648**, 28 (2007). hep-ex/0610021
24. M.N. Achasov et al. (SND Collaboration), JETP Lett. **103**, 380 (2006)

25. A. Quenzer et al. (DM1 Collaboration), Phys. Lett. B **76**, 512 (1978)
26. D. Bisello et al. (DM2 Collaboration), Phys. Lett. B **220**, 321 (1989)
27. S.J. Dolinsky et al. (ND Collaboration), Phys. Rep. C **202**, 99 (1991)
28. A. Cordier et al. (DM1 Collaboration), Nucl. Phys. B **172**, 13 (1980)
29. M.N. Achasov et al. (SND Collaboration), Phys. Rev. D **66**, 032001 (2002)
30. L.M. Barkov et al. (CMD Collaboration), Preprint INP 89-15, Novosibirsk (1989)
31. R.R. Akhmetshin et al. (CMD2 Collaboration), Phys. Lett. B **642**, 203 (2006)
32. M. Davier, S. Eidelman, A. Hoecker, Z. Zhang, Eur. Phys. J. C **27**, 497 (2003). hep-ph/0208177
33. M. Davier, S. Eidelman, A. Hoecker, Z. Zhang, Eur. Phys. J. C **31**, 503 (2003). hep-ph/0308213
34. S.J. Dolinsky et al. (ND Collaboration), Phys. Rep. C **202**, 99 (1991)
35. G. Cosme et al., Nucl. Phys. B **152**, 215 (1979)
36. C. Paulot, Ph.D. Thesis, Preprint LAL-79-14, Orsay, 1979
37. B. Esposito et al. (MEA Collaboration), Lett. Nuovo Cimento **28**, 195 (1980)
38. L.M. Barkov et al. (CMD Collaboration), Sov. J. Nucl. Phys. **47**, 248 (1988)
39. A. Cordier et al. (DM1 Collaboration), Phys. Lett. B **109**, 129 (1982)
40. A. Cordier et al. (DM1 Collaboration), Phys. Lett. B **81**, 389 (1979)
41. D. Bisello (for the DM2 Collaboration), Nucl. Phys. B **21**(Proc. Suppl.), 111 (1991)
42. D. Bisello et al. (DM2 Collaboration), Report LAL-90-35, Orsay (1990)
43. L. Stanco (for the DM2 Collaboration), in *Proceedings of Hadron-91, World Scientific ed. 84* (World Scientific, Singapore, 1992)
44. L.M. Kurdadze et al. (OLYA Collaboration), JETP Lett. **47**, 512 (1988)
45. R.R. Akhmetshin et al. (CMD2 Collaboration), Phys. Lett. B **466**, 392 (1999). hep-ex/9904024
46. M.N. Achasov et al. (SND Collaboration), Preprint BudkerINP 2001-34, Novosibirsk (2001)
47. M.N. Achasov et al. (SND Collaboration), J. Exp. Theor. Phys. **96**, 789 (2003)
48. G. Cosme et al. (M3N Collaboration), Nucl. Phys. B **152**, 215 (1979)
49. C. Paulot, Thesis, LAL-79-14, Orsay (1979)
50. L.M. Kurdadze et al. (OLYA Collaboration), JETP Lett. **43**, 643 (1986)
51. J. Burmester et al. (PLUTO Collaboration), Phys. Lett. B **66**, 395 (1977)
52. C. Berger et al. (PLUTO Collaboration), Phys. Lett. B **81**, 410 (1979)
53. L. Criegee, G. Knies, Phys. Rep. C **83**, 151 (1982)
54. Z. Jakubowski et al. (Crystal Ball Collaboration), Z. Phys. C **40**, 49 (1988)
55. C. Edwards et al. (Crystal Ball Collaboration), SLAC-PUB-5160 (1990)
56. J.Z. Bai et al. (BES Collaboration), Phys. Rev. Lett. **84**, 594 (2000). hep-ex/9908046
57. J.Z. Bai et al. (BES Collaboration), Phys. Rev. Lett. **88**, 101802 (2002). hep-ex/0102003
58. M. Ablikim et al. (BES Collaboration), Phys. Lett. B **641**, 145 (2006). hep-ex/0605105
59. M. Ablikim et al. (BES Collaboration), Phys. Lett. B **677**, 239 (2009). arXiv:0903.0900
60. A. Bäcker, Preprint DESY F33-77/03 (1977)
61. G. Bonneau, F. Martin, Nucl. Phys. B **27**, 381 (1971)
62. K. Nakamura et al. (Particle Data Group), J. Phys. G **37**, 075021 (2010)
63. A. Pais, Ann. Phys. **9**, 548 (1960)
64. K.G. Chetyrkin, J.H. Kühn, M. Steinhauser, Nucl. Phys. B **482**, 213 (1996). hep-ph/9606230
65. M. Davier, A. Hoecker, Phys. Lett. B **419**, 419 (1998). hep-ph/9801361
66. H. Flaecher, M. Goebel, J. Haller, A. Hoecker, K. Moening, J. Stelzer, Eur. Phys. J. C **60**, 543 (2009). arXiv:0811.0009. Updated results taken from: http://cern.ch/gfitter
67. F. Le Diberder, A. Pich, Phys. Lett. B **286**, 147 (1992)
68. A. Hoecker, W. Marciano, The muon anomalous magnetic moment, in: Particle Data Group (K. Nakamura et al.). J. Phys. G **37**, 075021 (2010)
69. T. Teubner, Talk given at Tau 2010 Workshop, Manchester, UK, 13–17 Sep 2010
70. K. Hagiwara, A.D. Martin, D. Nomura, T. Teubner, Phys. Lett. B **649**, 173 (2007). hep-ph/0611102
71. F. Jegerlehner, A. Nyffeler, Phys. Rep. **477**, 1 (2009). arXiv:0902.3360
72. J. Prades, E. de Rafael, A. Vainshtein, UG-FT-242-08, CAFPE-112-08, CPT-P092-2008, FTPI-MINN-08-41, UMN-TH-2723-08, (2009). arXiv:0901.0306
73. T. Kinoshita, M. Nio, Phys. Rev. D **73**, 013003 (2006). hep-ph/0507249
74. R. Jackiw, S. Weinberg, Phys. Rev. D **5**, 2396 (1972)
75. A. Czarnecki, W.J. Marciano, A. Vainshtein, Phys. Rev. D **67**, 073006 (2003). Erratum-ibid. D **73**, 119901 (2006). hep-ph/0212229
76. M. Knecht, S. Peris, M. Perrottet, E. de Rafael, J. High Energy Phys. **0211**, 003 (2002). hep-ph/0205102
77. A. Nyffeler, Phys. Rev. D **79**, 073012 (2009). arXiv:0901.1172
78. R. Alemany, M. Davier, A. Hoecker, Eur. Phys. J. C **2**, 123 (1998). hep-ph/9703220
79. S. Schael et al. (ALEPH Collaboration), Phys. Rep. **421**, 191 (2005). hep-ex/0506072
80. M. Fujikawa et al. (Belle Collaboration), Phys. Rev. D **78**, 072006 (2008). arXiv:0805.3773
81. S. Anderson et al. (CLEO Collaboration), Phys. Rev. D **61**, 112002 (2000). hep-ex/9910046
82. K. Ackerstaff et al. (OPAL Collaboration), Eur. Phys. J. C **7**, 571 (1999). hep-ex/9808019
83. M. Steinhauser, Phys. Lett. B **429**, 158 (1998). hep-ph/9803313